Journal of Solid State Chemistry **149,** 189–196 (2000)
Article ID jssc.1999.8521, available online at http://www.idealibrary.com on IDEAL®

Synthesis and Crystal Structure of a New Complex Oxyfluoride $La_{0.813}Sr_{0.187}Cu(O, F)_{3-\delta}$

A. M. Abakumov,* J. Hadermann,†,[1] M. G. Rozova,* B. Ph. Pavljuk,* E. V. Antipov,* O. I. Lebedev,†,[2] and G. van Tendeloo†

*Department of Chemistry, Moscow State University, 119899 Moscow, Russia; and †EMAT, University of Antwerp (RUCA), Groenenborgerlaan 171, B-2020 Antwerp, Belgium

Received August 10, 1999; in revised form September 14, 1999; accepted September 14, 1999

$La_{8-x}Sr_xCu_8O_{20-\delta}$ ($x = 1.3$, 1.5, and 1.9) compounds were fluorinated using XeF_2 as a fluorinating agent. The formation of a new tetragonal complex oxyfluoride $La_{0.813}Sr_{0.187}Cu(O, F)_{3-\delta}$ was observed. The structure of the new phase was refined using X-ray powder data ($a = 3.7921(3)$ Å, $c = 4.0515(4)$ Å, S. G. *P4/mmm*, $R_1 = 0.020$, $R_P = 0.045$, $R_{wP} = 0.057$) and was confirmed by electron diffraction and high-resolution electron microscopy (HREM). The tetragonal distortion of the perovskite unit cell seems to be due to a Jahn–Teller deformation of the copper coordination environment with the formation of four short (1.896 Å) and two long (2.026 Å) Cu–(O, F) distances. Domains of the $La_{0.813}Sr_{0.187}Cu(O, F)_{3-\delta}$ phase were observed by HREM inside a matrix of a slightly fluorinated initial phase.

Key Words: **fluorination; $La_{0.813}Sr_{0.187}Cu(O, F)_{3-\delta}$.**

1. INTRODUCTION

The structures of Cu-based high-temperature superconductors are commonly regarded as intergrowth structures of perovskite, rock salt, or fluorite-type blocks. The geometry of the (CuO_2) layers which are responsible for the transport properties of these compounds corresponds well to that of (BO_2) layers in ABO_3 perovskite. From this point of view the perovskite structure can be considered the simplest one suitable for superconductivity. Indeed, the oxygen-deficient "infinite layer" compound $SrCuO_2$ with stacking sequence -CuO_2-Sr-CuO_2- (compare with -BO_2-AO-BO_2- in perovskite) was converted to an *n*-type superconductor with $T_c = 40$ K by appropriate electron doping using partial replacement of Sr by La (1).

Besides the two-dimensional "infinite layer" compounds, a large variety of three-dimensional anion-deficient perovskites are known (2–15). The structures of these compounds are varied mainly by the ordering of oxygen atoms and anion vacancies in the *a–b* plane of the perovskite subcell: rows of oxygen atoms parallel to the [001] direction are eliminated in an ordered manner, leaving hexagonal channels and decreasing the copper coordination number from 6 to 5, 4, or 2. The concentration of anion vacancies and their ordering can be changed by variation of the ratio between trivalent and bivalent A-cations and the partial oxygen pressure during thermal treatments. These compounds show metallic or semiconducting behavior, but superconductivity has never been observed due to the absence of (CuO_2) layers or the three-dimensional character of the structure.

The stoichiometric distorted perovskite $LaCuO_3$ does not exhibit superconductivity due to the high formal valence of the Cu atoms ($V_{cu} = +3$) (16, 17). It is interesting to consider the possibility of exchanging O^{2-} anions by F^- ones to achieve a reduction of the copper atoms. The $LaCuO_2F$ hypothetic compound with a stacking sequence -CuO_2-LaF-CuO_2- can be chosen as a starting point of $La_{1-x}Sr_xCuO_2F$ solid solutions, where the copper oxidation state is varied by heterovalent cation replacement. However, the preparation of such compounds by direct solid state reaction of oxides and fluorides is hampered by the high thermodynamic stability of SrF_2 and LaOF. In this case it is necessary to apply a soft chemistry technique of fluorination of the parent compounds with appropriate cation ratio (La, Sr)/Cu = 1. In this work we describe the fluorination of $(La_{1-x}Sr_x)_8Cu_8O_{20-\delta}$ using XeF_2 as a soft fluorinating agent. The initial compounds have a tetragonal structure ($a \approx a_p2\sqrt{2}$ and $c \approx a_p$; a_p is the parameter of the perovskite subcell) (10, 11), where copper atoms adopt octahedral, pyramidal, and square planar coordinations. Since (CuO_2) planes are absent in the initial structure, an anion rearrangement is necessary for the formation of a two-dimensional structure containing (CuO_2) planes and the appearance of superconducting properties. It is possible to

[1]To whom correspondence should be addressed. Fax: +32/32180257.
[2]On leave from the Institute of Crystallography, RAS, Leninsky prospekt 59, 117333, Moscow, Russia.

0022-4596/00 $35.00

expect such a structural transformation under fluorination of these anion-deficient perovskites. An example of successful anion rearrangement from one-dimensional chains of CuO_4 squares to two-dimensional (CuO_2) layers was provided by the fluorination of Sr_2CuO_3, which converts this compound into the $Sr_2CuO_2F_{2+\delta}$ superconductor with $T_c = 46$ K (18).

2. EXPERIMENTAL

Single-phase samples corresponding to three points of the $La_{8-x}Sr_xCu_8O_{20-\delta}$ ($x = 1.3$, 1.5, and 1.9) solid solution were prepared by a routine ceramic technique using La_2O_3, $SrCO_3$, and CuO as initial reagents. Stoichiometric amounts of the starting materials were ground in an agate mortar under acetone and pressed into pellets. The samples were annealed at 850°C for 60 h, then at 1000°C for 48 h in air and then furnace cooled. The copper formal valence for all samples was determined by iodometric titration. The oxygen off-stoichiometry δ was found to be $\delta = 0.29$ ($x = 1.3$), $\delta = 0.35$ ($x = 1.5$), and $\delta = 0.41$ ($x = 1.9$).

All operations with XeF_2 were carried out in a glove box filled with dried N_2. First, 0.4 g of the initial material was mixed with XeF_2 (provided by the Laboratory of Inorganic Synthesis of the Institute of Applied Chemical Physics "Kurchatovskii Institut," Moscow, Russia) in a molar ratio of 1–2 and ground in an agate mortar. The mixture was placed in an Ni-crucible and then sealed into an N_2-filled copper tube. The samples were annealed at temperatures ranging from 300 to 400°C for 30–50 h and furnace cooled to room temperature.

The phase composition of the samples and the lattice parameters of the compounds were determined by X-ray diffraction using a focusing Guinier-camera FR-552 ($CuK\alpha_1$-radiation, germanium internal standard). Raw data for structure refinement were collected using a Philips X'pert diffractometer ($CuK\alpha$-radiation, reflection geometry, proportional counter, angular range 15–100° 2θ, step 0.02°).

The RIETAN-97 (20) program was used for powder crystal structure refinement. The final refinement was carried out by the Rietveld method with a pseudo-Voigt profile function.

AC susceptibility measurements were performed in the temperature range 12–100 K at an external field amplitude of 1 Oe and a frequency of 27 Hz.

High-resolution electron microscopy (HREM) observations were performed using a JEOL 4000EX microscope. The qualitative EDX analysis and electron diffraction (ED) study were made using a Philips CM20 microscope with a LINK-2000 attachment.

TABLE 1
Phase Compositions and Cell Parameters of the Compounds in Initial and Fluorinated Samples

No.	Fluorination conditions	a (Å)	c (Å)
1	$La_{6.7}Sr_{1.3}Cu_8O_{19.71}$, initial (I)	10.842(2)	3.8654(9)
2	$La_{6.5}Sr_{1.5}Cu_8O_{19.65}$, initial (II)	10.8340(8)	3.8617(5)
3	$La_{6.1}Sr_{1.9}Cu_8O_{19.59}$, initial (III)	10.814(1)	3.8606(6)
4	I : XeF_2 = 1 : 1, 300°C, 30 h, phase A	10.832(1)	3.8677(7)
5	I : XeF_2 = 1 : 2, 300°C, 30 h		
	Phase A	10.8342(9)	3.8683(7)
	Phase B	3.7916(7)	4.044(1)
6	II : XeF_2 = 1 : 2, 300°C, 50 h		
	Phase A	10.829(2)	3.866(1)
	Phase B	3.7918(8)	4.0537(9)
7	III : XeF_2 = 1 : 2, 400°C, 50 h, phase A	10.8275(7)	3.8684(4)

3. RESULTS

3.1. Phase Compositions

Fluorination conditions, phase compositions, and cell parameters of the initial and some fluorinated compounds are listed in Table 1.

The phase compositions and cell parameters of the compounds observed in the fluorinated samples depend on the amount of XeF_2 in the starting mixture, on the fluorination temperature, and on the composition of the initial compounds. In all samples a phase with cell parameters close to those for the initial phases (phase A) was observed. Cell parameters for phase A do not change significantly in comparison with the initial compound: a small decrease of a and an increase of the c parameter was found for almost all samples fluorinated at 300°C except sample 7, obtained at 400°C. The compound in this sample shows an increase of the a parameter.

The important feature of samples 5 and 6 is the presence of a new tetragonal phase (phase B) with cell parameters clearly connected with the cell parameters of the initial phase and the perovskite subcell: $a \approx a_{ini}/2\sqrt{2} \approx a_p$, $c \approx c_{ini} \approx a_p$ (a_{ini} and c_{ini} are the cell parameters of the initial phase). This phase is always present in the samples together with phase A. The amount of phase B changes upon variation of fluorination conditions, but all our attempts to prepare phase B without admixture of phase A were unsuccessful. Figure 1a reproduces the X-ray diffraction pattern of sample 6, where the reflections of phase B are marked by arrows. After this sample is heated in air at 400°C for 20 h this phase decomposes, leaving reflections of phase A and broad reflections corresponding to badly crystallized LaOF and SrF_2 (Fig. 1b). Annealing in air also results in an increase of the a and c cell parameters of phase A: $a = 10.8478(7)$ Å, $c = 3.8791(3)$ Å. Figure 1c represents the diffraction pattern of phase B obtained by subtraction of the

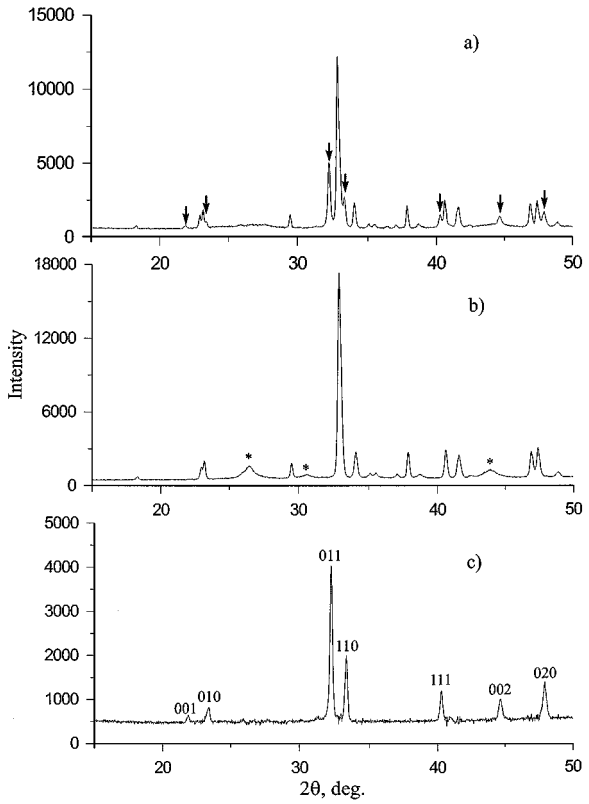

FIG. 1. The X-ray diffraction patterns for sample 6: fluorinated (a), annealed at 400°C in air (b), pattern of the B phase (c). The reflections of the B phase are marked by arrows; the broad peaks from badly crystallized LaOF and SrF_2 are marked by asterisk.

reflections of phase A by profile fitting using their known positions and intensities.

The measurements of the temperature dependence of the magnetic susceptibility revealed only weak paramagnetism and an absence of superconductivity down to 12 K for the fluorinated as well as for the initial samples.

3.2. Crystal Structures

Since the B phase was obtained only in a mixture with the A phase we attempted to calculate both crystal structures using a two-phase Rietveld refinement procedure. The diffraction peaks of phase B in Fig. 1c show an intensity distribution typical for a tetragonally distorted perovskite-like structure. According to that, the starting model was based on a tetragonally distorted perovskite unit cell, where La and Sr atoms are randomly distributed over the A-positions and where the B-positions are occupied by Cu atoms. Since O and F have the same scattering power, they were refined as oxygen atoms placed at the middle of each unit cell edge. The *P*4/*mmm* space group was chosen for the refinement as the most symmetrical tetragonal space group without extinction conditions. The atomic coordinates for

TABLE 2
Parameters of the Rietveld Refinement of the Crystal Structures of the A and B Phases

Phase	A	B
Space group	*P*4/*mbm*	*P*4/*mmm*
a (Å)	10.8269(4)	3.7921(3)
c (Å)	3.8665(2)	4.0515(4)
Cell volume (Å^3)	453.24(3)	58.261(9)
Calculated density (g/cm^3)	6.820	6.861
Mass fraction in the sample	0.67	0.33
Number of reflections	151	31
Refineable parameters	19	9
R_I	0.025	0.020
R_P, R_{wP}	0.045, 0.057	

phase A were taken from the $La_{6.4}Sr_{1.6}Cu_8O_{19.84}$ crystal structure (11). The refinement of the occupancies of all possible anion positions for the structure of the A phase gave values close to 1.0 except for the 0.125, 0.625, 0 position. The occupation factor for this position dropped to 0.0, and it was assumed to be vacant. It should be noted that the occupancies correlate very strongly with the thermal parameters, and they were fixed to 1.0 to overcome the correlation effects. This did not change either atomic coordinates or reliability factors. For phase B the refined occupancies were 0.95(4) and 0.82(3) for O(1) and O(2), respectively. However, the reliability factors were insensitive to a variation of the occupancies, and they were also fixed to be equal to 1.0. The final refinement was made with an overall thermal parameter for all atoms of the B structure. For phase A the thermal parameters were separated into three different blocks for La(Sr), Cu, and oxygen atoms, respectively. The final values of the reliability factors reflect that good agreement between experimental and calculated profiles was achieved: $R_{1(A)} = 0.025$, $R_{1(B)} = 0.020$, $R_P = 0.045$, $R_{wP} = 0.057$. The parameters of the Rietveld refinement, the atomic coordinates, and the main interatomic distances for phases A and B are listed in Tables 2, 3, and 4, respectively. Experimental, calculated, and difference X-ray profiles are shown in Fig. 2.

3.3. Electron Microscopy Study

The results obtained using X-ray diffraction were further supported and completed by electron microscopy investigation. The [001]* diffraction patterns (DP) of phases A and B are shown in Fig. 3. The brighter spots on both patterns correspond to a perovskite subcell with $a_p \approx 3.8$ Å. No additional reflections were found on the [001]* DP of phase B, whereas the [001]* DP of phase A exhibits a square array of weaker spots corresponding to a $a = b \approx a_p 2\sqrt{2}$ superstructure. Note the splitting of basic spots along the [110]

TABLE 3
Positional and Thermal Parameters for the B Crystal Structure

Atom	Position	x	y	z	B_{iso} (Å^2)
La(Sr)[a]	1(*d*)	1/2	1/2	1/2	1.6(2)
Cu	1(*a*)	0	0	0	1.6(2)
O(1)	2(*f*)	0	1/2	0	1.6(2)
O(2)	1(*b*)	0	0	1/2	1.6(2)

[a]La(Sr) = 0.813La + 0.187Sr.

TABLE 4
Selected Interatomic Distances for the B Structure (Å)

La(Sr)–O(1)	2.7746(4) × 8	Cu–O(1)	1.8960(3) × 4
La(Sr)–O(2)	2.6814(3) × 4	Cu–O(1)	2.0258(4) × 2

direction, arising due to inclusions of phase B, which has a larger interplanar spacing in the $[110]_A = [001]_B$ direction.

Only seldom were found separate crystallites containing only the B phase. Phase B almost always coexists alongside phase A in one crystallite. HREM observations allowed us to differentiate the phases A and B. It should be noted that the projections of the A and B structures are very close since they differ from each other only by the concentration and distribution of anion vacancies. Both structures produce similar contrast under HREM conditions but can be easily distinguished using computer-calculated Fourier transforms of the HREM images. Figure 4 shows both phases, as well as the interface between a $[001]_A$ and a $[010]_B$ area. The $[001]_A$ area exhibits a periodic wavelike distortion of the rows of dots and an alternation of the brightness of dots corresponding to the projections of different Cu–O columns. The Fourier transform (at the bottom of Fig. 4) confirms that this periodicity belongs to the $a \approx b \approx a_p 2\sqrt{2}$ supercell. The contrast observed on the $[010]_B$ area agrees well with the structure of phase B, and the Fourier transform of this part of the image does contain the superstructure reflections. The correspondence between HREM images and calculated A and B crystal structures was also verified using image simulations which are in good agreement with the experimentally observed image contrast. Figure 5 shows the interface between a $[110]_A$ and a $[001]_B$ area. In the area of phase A the repeat period along $[\bar{1}10]_A = [100]_B$ corresponds to the spacing between the rows of brightest dots, and it is clearly twice as large as the

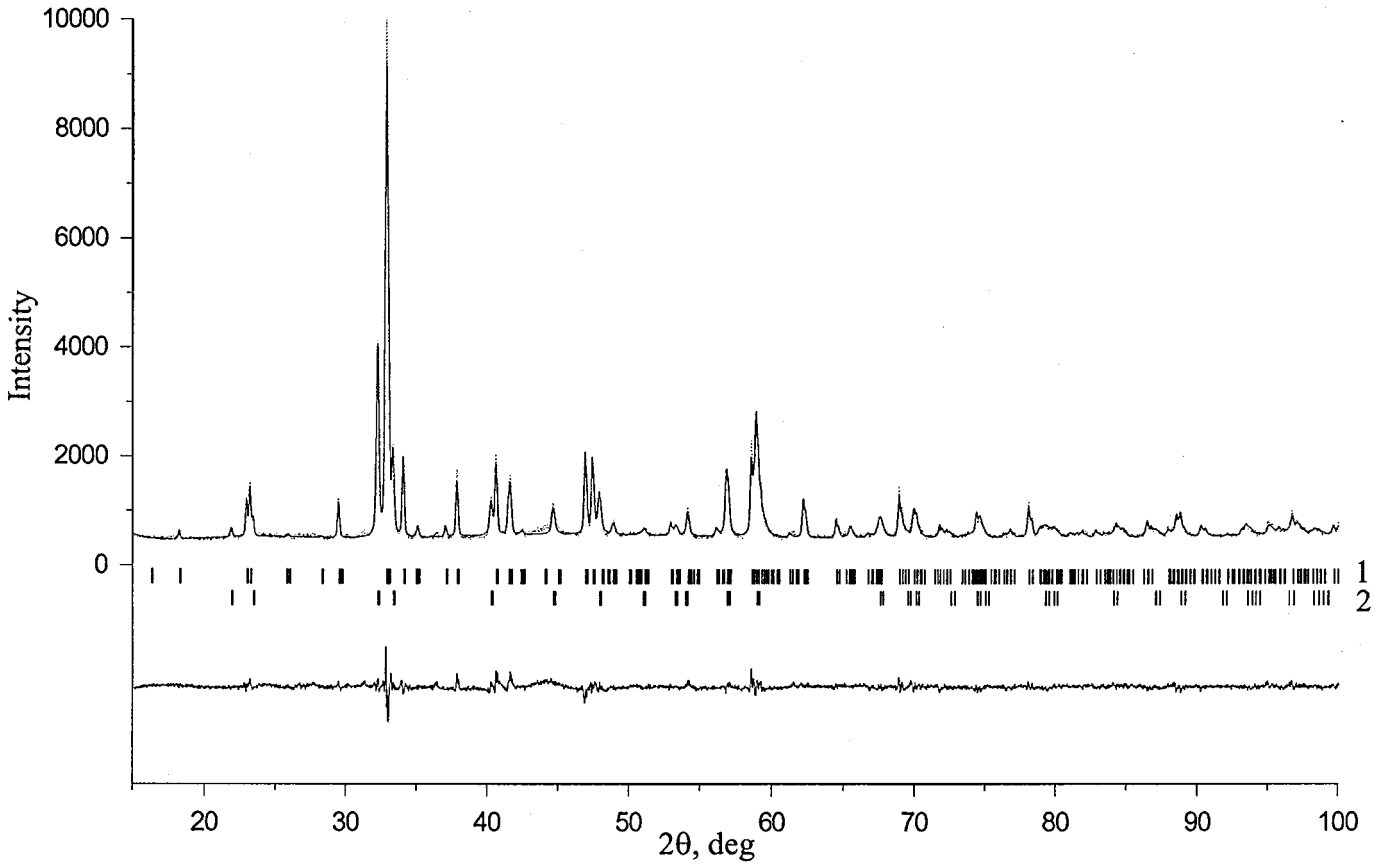

FIG. 2. Experimental, calculated, and difference X-ray profiles for the simultaneous refinement of A and B crystal structures.

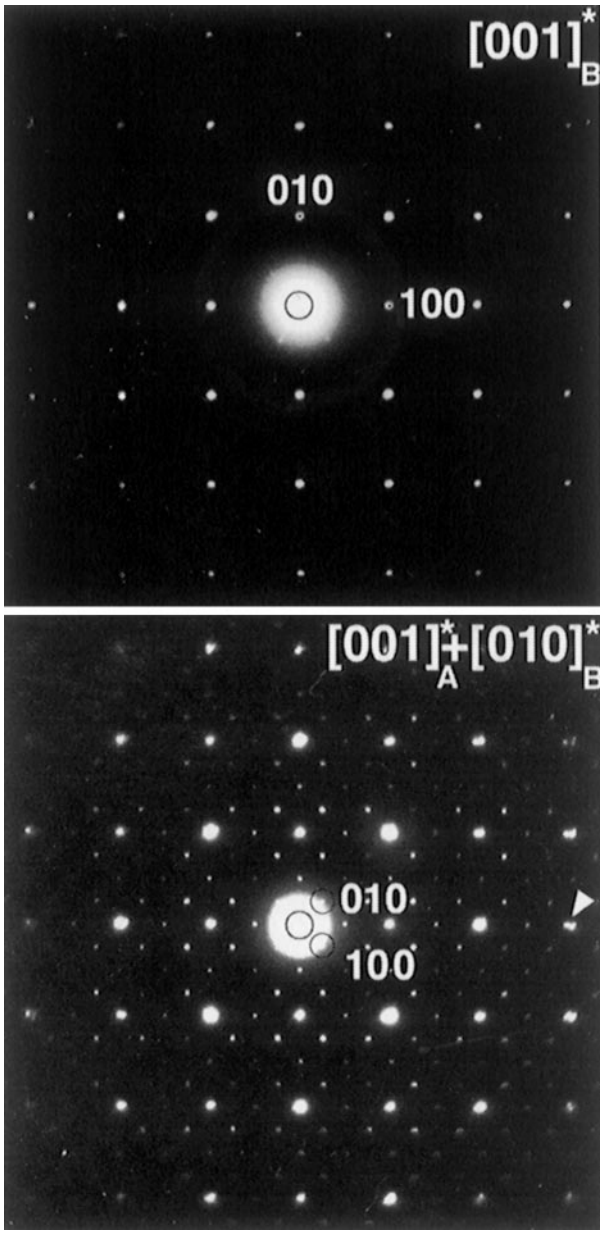

FIG. 3. Electron diffraction patterns taken from the $[001]_B$ and $[001]_A + [010]_B$ regions.

repeat period in the area of phase B. This difference is also reflected by the Fourier transforms which are shown at the right in Fig. 5. According to the HREM observations one can conclude that the domains of phase B grow at the expense of the A phase, and the mutual orientation of the tetragonal lattices in both domains is given by the relations $[100]_B = [\bar{1}10]_A$, $[010]_B = [001]_A$, and $[001]_B = [110]_A$. The interfaces between the adjacent domains are not well defined, are randomly oriented, and do not have a certain crystallographic orientation.

A qualitative EDX analysis was performed to determine the presence of fluorine in phases A and B. Figure 6 reproduces parts of the EDX spectra containing O($K\alpha$) and F($K\alpha$) peaks. The measurements revealed only traces of fluorine in the crystallites of phase A (Fig. 6a), whereas the crystallites of the B phase contain a significant amount of fluorine (Fig. 6b). One cannot exclude, however, the possibility that the fluorine found in the crystallites of phase A could be due to the presence of small areas of phase B inside these crystallites. Under our particular experimental conditions (EELS being installed on a 300kV FEG microscope), the performance of quantitative measurements of O and F using EELS-analysis is not possible, due to the instability of this compound under irradiation by a high-intensity electron beam.

4. DISCUSSION

The X-ray diffraction and electron microscopy studies clearly reveal significant transformations in structure and phase composition occurring after fluorine insertion into the vacant anion sites of the perovskite-like three-dimensional structure of $La_{8-x}Sr_xCu_8O_{20-\delta}$. The fluorination results in a phase separation with the formation of a new

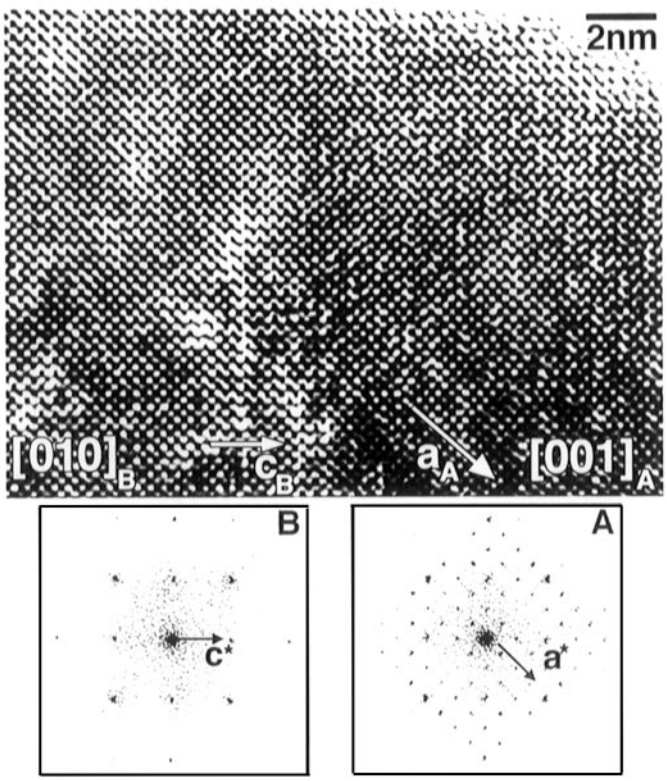

FIG. 4. HREM image of the interface between the $[001]_A$ and $[010]_B$ domains. The Fourier transforms from the A and B regions are shown at the bottom.

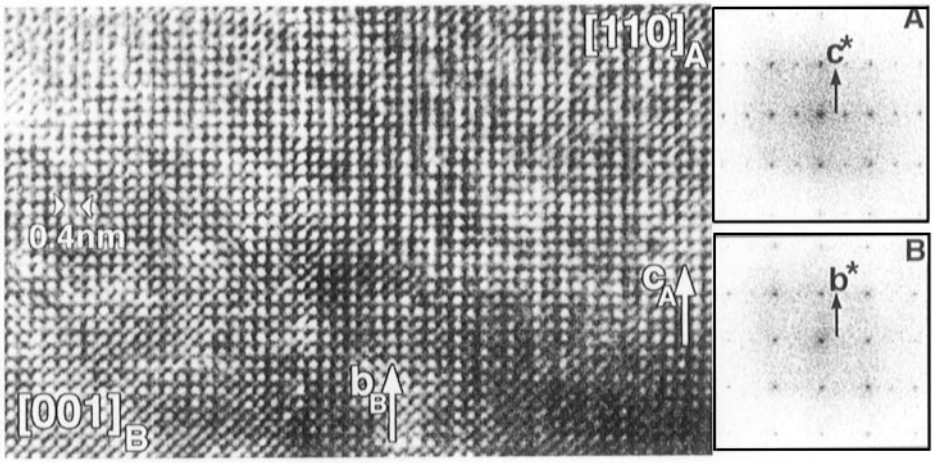

FIG. 5. HREM image of the interface between the $[001]_B$ and $[110]_A$ domains. The Fourier transforms from the A and B regions are shown at the right.

tetragonal perovskite phase (called B). The appearance of this phase, as well as its content in the sample, strongly depends on the fluorination conditions. The most probable chemical reaction during the fluorination can be expressed by the equation

$$\mathrm{La_{6.5}Sr_{1.5}Cu_8O_{19.65}} + 4(x+y)\mathrm{XeF_2} = 8\mathrm{La_{0.813}Sr_{0.187}CuO_{2.46-}}_x\mathrm{F}_x\mathrm{F}_y + 4(x+y)\mathrm{Xe} + 8x[\mathrm{O}].$$

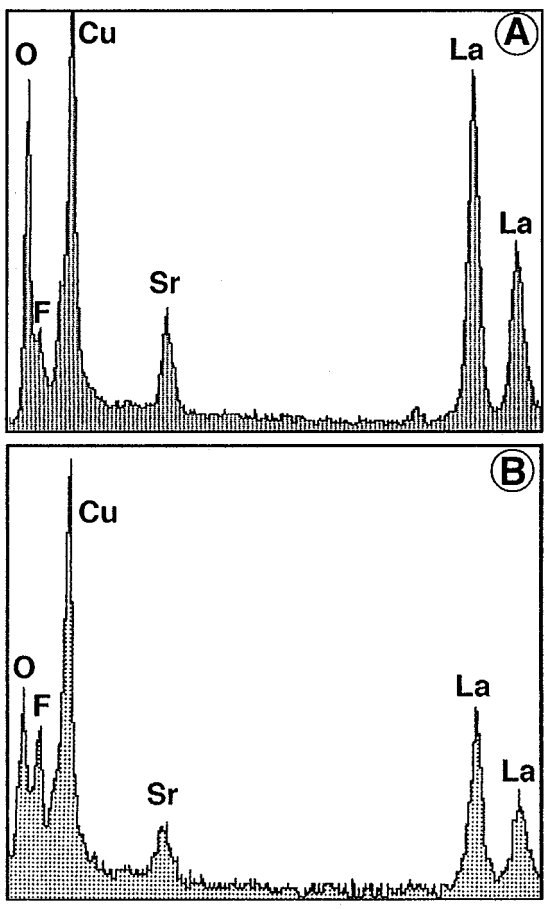

FIG. 6. Parts of the EDX spectra containing O($K\alpha$) and F($K\alpha$) peaks taken from regions of phase A (A) and phase B (B).

This implies that both the fluorine insertion and the anion exchange take place under fluorination, resulting in uncertainties in anion composition and copper oxidation state in the reaction products. The oxygen released due to anion exchange is absorbed by the inner walls of the Cu tube. The formation of phase B requires a relatively high concentration of XeF_2 which significantly exceeds the amount of extra anions which the initial structure can accommodate. The phase separation can be assumed to be a result of the restricted diffusion ability of the gaseous fluorinating agent at low fluorination temperature, and a high vapor pressure of XeF_2 can be a necessary condition to achieve the appropriate concentration of the fluorinating agent inside the crystallites. Increasing the temperature suppresses the formation of the B phase (Table 1, sample 7). Anion exchange becomes the main reaction at elevated temperatures and leads to the replacement of oxygen by fluorine with a partial reduction of copper. The increase of the a parameter for the A phase after fluorination at 400°C confirms this assumption.

A high fluorine content in the B phase was observed by EDX and was also confirmed by the appearance of LaOF and SrF_2 as main products of the decomposition of this phase after annealing in air. Phase A is probably also affected by fluorination, but the fluorine content in this phase is much lower than that in phase B. The small

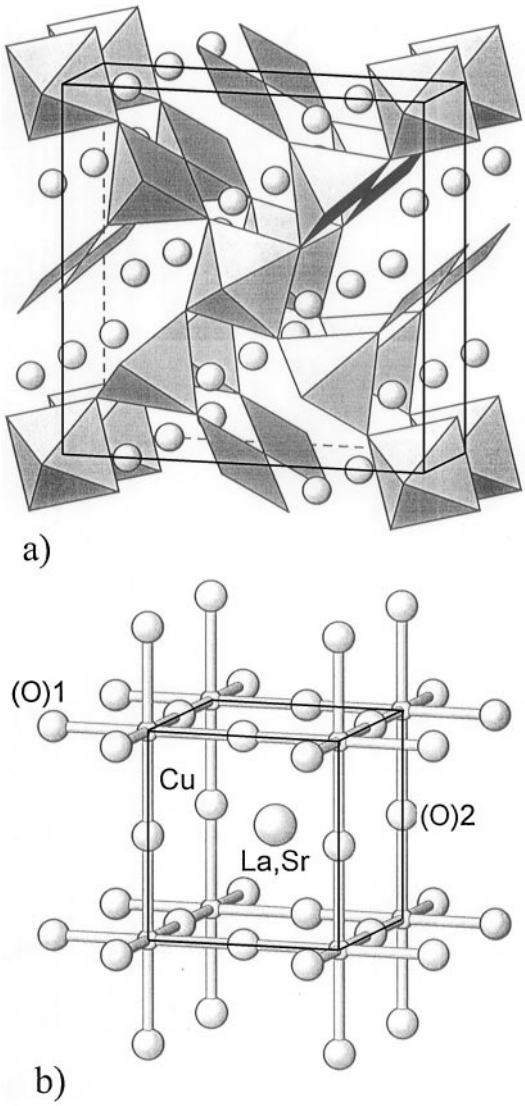

FIG. 7. The crystal structures of phases A (A) and B (B). For phase A the copper atoms are inside squares, pyramids, and octahedra. For phase B the framework of Cu–(O, F) bonds is shown. La(Sr) atoms are imaged as shaded large circles.

decrease of the *a* parameter for this phase can be explained by contraction of Cu–O bonds due to the increase of the formal copper valence by fluorine insertion. The air-annealed fluorinated phase A has an *a* parameter even slightly larger than that of the initial compound, which can be explained by a loss of extra anions with a reduction of copper atoms.

The crystal structures of the A and B phases are presented in Fig. 7. The atomic coordinates and La(Sr)–O and Cu–O distances for phase A are very similar to those previously published for the structure of the $La_{6.4}Sr_{1.6}Cu_8O_{19.84}$ compound (11). No additional occupied anion sites were found in the structure of phase A. Since the occupancies of the anion positions were close to 1.0, one can assume that the anion vacancies corresponding to the oxygen nonstoichiometry $\delta = 0.35$ for the initial material are filled by fluorine in the structure of the A phase. However, the results of Rietveld refinement do not allow us to evaluate the exact amount of inserted fluorine or the distribution of extra anions between the different positions.

In the tetragonally distorted perovskite-like structure of the B phase, all possible anion positions are partially or fully occupied by oxygen and fluorine atoms. According to this the $La_{0.813}Sr_{0.187}Cu(O, F)_{3-\delta}$ composition can be proposed for this phase. Using the values of the occupancy factors obtained after the Rietveld refinement one can assume that the anion vacancies are preferentially located at the apical sites of the copper coordination polyhedra, whereas the equatorial positions in the $Cu(O, F)_2$ layers are probably fully occupied. An octahedral environment for at least part of the copper atoms results in a Jahn–Teller deformation of the copper coordination with the formation of four short (1.896 Å) and two long (2.026 Å) Cu–(O, F) distances. The apical elongation of the Cu–(O, F) octahedra leads to a tetragonal distortion of the perovskite structure. The tetragonal unit cell of $La_{0.813}Sr_{0.187}Cu(O, F)_{3-\delta}$ can be compared with the unit cell parameters for the tetragonal high-pressure form of $LaCuO_3$ (19) and the anion-deficient $LaCuO_{2.95}$ (21). In these cases all copper atoms have a formal valence equal or close to $+3$, and no Jahn–Teller effect can be observed for their octahedral environment. Indeed, the difference between the parameters of the perovskite subcell along the *a*- and *c*-directions is much smaller in $LaCuO_3$ (3.840 and 3.918 Å) and $LaCuO_{2.95}$ (3.819 and 3.972 Å) than in $La_{0.813}Sr_{0.187}Cu(O, F)_{3-\delta}$ (3.792 and 4.052 Å). The absence of superconducting properties for the $La_{0.813}Sr_{0.187}Cu(O, F)_{3-\delta}$ phase can be explained by a possible overdoping or partial occupation of the anion positions in the conducting layers by fluorine atoms, causing charge localization.

ACKNOWLEDGMENTS

This work was partially supported by the Russian Council on Superconductivity (Poisk), Intas-932483ext, RFBR (98-15-96058), and RFBR-INTAS (00639 I-96). A.A. and O.L. are grateful to the DWTC and the FWO (Belgium), respectively, for financial support during their stay at the University of Antwerp. This work has been performed within the framework of IUAP 4/10. The authors are grateful to Dr. P. Kazin for magnetic measurements.

REFERENCES

1. M. G. Smith, A. Manthiram, J. Zhou, J. B. Goodenough, and J. T. Markert, *Nature* (*London*) **351,** 549 (1991).
2. C. Michel, L. Er Rakho, M. Hervieu, J. Pannetier, and B. Raveau, *J. Solid State Chem.* **68,** 143–152 (1987).
3. C. Michel, L. Er Rakho, and B. Raveau, *Mater. Res. Bull.* **20,** 667–671 (1985).

4. R. Vijayaraghavan, R. A. Moham Ram, P. Ganguly, and C. N. R. Rao, *J. Solid State Chem.* **78,** 316–318 (1989).
5. R. Vijayaraghavan, R. A. Moham Ram, P. Ganguly, and C. N. R. Rao, *Mater. Res. Bull.* **23,** 719–723 (1988).
6. M. Kato, N. Kojima, K. Yoshimura, Y. Ueda, N. Nakayama, K. Kosuge, Z. Hiroi, and Y. Bando, *J. Solid State Chem.* **103,** 253–262 (1993).
7. N. Rangavittal, G. N. Subbana, T. N. Guru Row, and C. N. R. Rao, *J. Solid State Chem.* **114,** 95–101 (1995).
8. P. K. Davies and C. M. Katzan, *J. Solid State Chem.* **88,** 368–383 (1990).
9. K. Otzschi, A. Hayashi, Y. Fujiwara, and Y. Ueda, *J. Solid State Chem.* **105,** 573–579 (1993).
10. K. Otzschi and Y. Ueda, *J. Solid State Chem.* **107,** 149–158 (1993).
11. L. Er Rakho, C. Michel, and B. Raveau, *J. Solid State Chem.* **73,** 514–519 (1988).
12. W. T. Fu, D. J. W. Ijdo, and R. B. Helmholdt, *Mater. Res. Bull.* **27,** 287–293 (1992).
13. W. T. Fu, Q. Xu, A. A. Verheijen, J. M. van Ruitenbeek, H. W. Zandbergen, and L. J. de Jongh, *Solid State Commun.* **73,** 291–295 (1990).
14. W. T. Fu, F. C. Mijlboff, D. J. W. Ijdo, and V. Ponec, *Solid State Commun.* **83,** 59–62 (1992).
15. K. Otzschi, K. Koga, and Y. Ueda, *J. Solid State Chem.* **115,** 490–498 (1995).
16. G. Demazeau, C. Parent, M. Pouchard, and P. Hagenmuller, *Mater. Res. Bull.* **7,** 913 (1972).
17. A. W. Webb, E. F. Skelton, S. B. Quadri, E. R. Carpenter Jr., M. S. Osofsky, R. J. Soulen, and V. Letourneau, *Phys. Lett. A* **137,** 205–206 (1989).
18. M. Al-Mamouri, P. P. Edwards, C. Greaves, and M. Slaski, *Nature* (*London*) **369,** 382–383 (1994).
19. J. F. Bringley, B. A. Scott, S. J. La Placa, T. R. MgGuire, and F. Mehran, *Phys. Rev. B* **47**(22), 15269–15275 (1993).
20. Izumi F., *in* "The Rietveld Method" (R. A. Young, Ed.), Chap. 13. Oxford University Press, Oxford, 1993.